

Mixing state of ~~refractory~~ black carbon at different atmospheres in north and south west China

Gang Zhao¹, Tianyi Tan¹, Shuya Hu¹, Zhuofei Du¹, Dongjie Shang¹, Zhijun Wu^{1,2}, Song Guo^{1,2}, Jing Zheng¹, Wenfei Zhu¹, Mengren Li¹, Limin Zeng¹, Min Hu^{1, 2*}

1 State Key Joint Laboratory of Environmental Simulation and Pollution Control, International Joint Laboratory for Regional Pollution Control, Ministry of Education, College of Environmental Sciences and Engineering, Peking University, Beijing, 100871, China

2 Collaborative Innovation Center of Atmospheric Environment and Equipment Technology, Nanjing University of Information Science & Technology, Nanjing, China

*Correspondence author: Min Hu (minhu@pku.edu.cn)

Abstract

~~Black carbon (BC) particles exert a significant influence on the earth's climate system. However, l~~large uncertainties remain when estimating the radiative forcing by black carbon (BC) because the corresponding microphysical properties have not been well addressed. ~~Knowledge of the BC mixing states of different aging degree can help better characterise the corresponding environmental and climate effects.~~ In this study, the BC size distributions were studied based on three different field campaigns at an urban site, a suburban site, and a background site in China using a single particle soot photometer (SP2) in tandem with a differential mobility diameter. Measurement results ~~from the SP2~~ indicates that the BC particles were composed of either fresh-thinly or aged-thickly coated aerosols. The mean number fractions of the fresh-thinly coated BC aerosols were 51%, 67%, and 21% for the urban, suburban, and background sites,

respectively. ~~The corresponding mobility diameters of these aged thickly coated (fresh thinly coated) BC-containing aerosols were 294 nm (193 nm), 244 nm (161 nm), and 257 nm (162 nm). The measured aged thickly coated (fresh thinly coated) BC core number median diameters were 115 nm (114 nm), 107 nm (95 nm), and 127 nm (111 nm) for urban, suburban, and background sites, respectively.~~ The corresponding aged thickly coated (fresh thinly coated) core mass median diameters were 187 nm (154 nm), 182 nm (146 nm), and 238 nm (163 nm) respectively. The mean diameter of the aged thickly coated BC-containing aerosols was larger than that of the fresh thinly coated BC-containing aerosols, while the mean BC core diameter of the aged thickly coated BC-containing aerosols was smaller than that of the fresh thinly coated BC-containing aerosols. About 10% of the BC-containing aerosols with the BC core ~~were~~ attached to the other non-BC components, which were mainly generated by coagulation between the BC and non-BC components. The measurement results in our study can ~~help better understand the BC size distributions and mixing status in the different atmospheres in China and~~ can be further used in modeling studies to help constrain the uncertainties of the BC radiative effects.

Introduction

Black carbon (BC) plays an important role in the climate system by absorbing solar radiation (Ramanathan and Carmichael, 2008), interacting with the cloud (Roberts et al., 2008), and changing the albedo of the snow (Menon et al., 2002). It is the second most important aerosol component after carbon dioxide, contributing to global warming (Bond et al., 2013). The solar absorption of BC has a significant influence on the development of the boundary layer and then aggravates the air pollution (Ding et al., 2016). The turbulence in the atmospheric boundary layer can be suppressed due to the existence of BC (Wilcox et al., 2016). The BC also plays a remarkable role in driving the formation and trend of regional haze (Zhang et al., 2020).

BC is mainly generated by the incomplete combustion of biofuels and fossil fuels (Bond and Bergstrom, 2006). After emission, the morphology of BC transforms from fractal to spherical and subsequently grows to a fully compact particle with other chemical components coating on it (Peng et al., 2016). During the aging process, the BC optical properties change significantly up to a factor of 3 and then the corresponding magnitude of climate forcing contributed by BC is increased by up to a factor of 2 (Zhang et al., 2008). Large uncertainties remain in estimating the BC radiative effects due to the large variation in BC microphysical properties, such as size distributions and mixing states during the aging process (Zhao et al., 2019; Moffet et al., 2016; Matsui et al., 2018). Therefore, characterizing the differences in size distributions and mixing states between the thinly and thickly coated ~~fresh and aged~~ BC particles can help better constrain the uncertainties of BC aerosol radiative effects. To our best understanding, few studies have specified the mixing states and size distributions of both the thinly and thickly coated ~~fresh and aged~~ BC aerosols.

The thickly coated ~~BC-containing~~ particles can also be classified into two morphological types: bare BC on the surface of non-BC particles or partially coated by non-BC particles (attached type) and BC embedded within or coated by non-BC components (coated type). With the same amount of non-BC components, the mass absorption cross-sections of BC by the attached type are much smaller than those by the coated type (Moteki and Kondo, 2008; Moteki and Kondo, 2010; Moteki et al., 2014). Therefore, the impact of BC on climate can be better estimated when accurately identifying the two types of ambient BC-containing particles. Observations are required to constrain the spatial and temporal microphysical properties of the atmospheric BC.

The single-particle soot photometer (SP2) is always used to measure the mixing states and size distributions of ambient BC particles. In the previous study, the advanced technique were used to study the coating over different BC core size diameter on the

ground (Liu et al., 2019a) and for vertical profiles (Ding et al., 2019). The measured signals from SP2 can be used to distinguish the BC-containing aerosols as ~~fresh~~-thinly and ~~aged~~-thickly coated ones. The measured results can also be employed to distinguish the BC-containing particles between attached and coated types, which were described in detail in the methodology part.

In this study, the tandem SP2 and differential mobility analyzer (DMA) was employed at an urban site, a suburban site, and a background site in China to investigate the microphysical properties of the BC particles. The size distributions and mixing states of both the ~~fresh~~ thinly coated and ~~aged~~ thickly coated BC aerosols at different atmospheres were characterized. We also investigated the corresponding morphology properties of the BC-containing aerosols. The measured microphysical properties provide the basis for future modeling studies of the BC radiative effects of different environment in China.

2 Methodology

2.1 Measurement sites

The measurements were conducted at three different atmospheric sites in China, namely the urban site of Peking University Urban Atmosphere Environment Monitoring Station (PKU, 39.9°N, 116.1°E, 58m a.s.l) in Beijing between 20 January and 4 February 2016, the suburban site of Changping (CP, 40.3°N, 116.2°E, 70m a.s.l) in Beijing between 15 May and 5 June 2016, and the background site of Lijiang (LJ, 27.2°N, 100.2°E, 3410 m a.s.l) in Yunnan Province between 22 March and 4 April 2015. The PKU site is located in the northwest of Beijing. This site could characterize the air pollution of the urban Beijing (Hu et al., 2017; Hu et al., 2021b). The CP site locates at the northwest of the Beijing urban area, representing a regional atmosphere (Zhao et al., 2021; Wang et al., 2019b). The LJ site represents the background areas, located in the

101 Mountain Yulong, in the Yunan Province of China (Shang et al., 2018; Zheng et al.,
102 2017; Wang et al., 2019a). The aerosol optical depth at the wavelength of 550 nm during
103 the year 2020 indicated that the LJ site was very clean and the PKU and CP sites were
104 more polluted as shown in Fig. S1 in the supplement.

105 **2.2 Instruments**

106 **2.2.1 DMA-SP2 system**

107 As for the SP2, the continuous Nd: YAG laser beam with the wavelength of 1064
108 nm is generated intensively in the instrument chamber. When the BC-containing
109 particles pass through the laser beam, they absorb the radiation and then are heated to
110 around 3500-5000 K. The intensity of the emitted incandescent light from the heated
111 BC particle is then transformed to the BC mass concentration. The scattering signals of
112 the BC particle are recorded to estimate the BC particle mixing state.

113 In this study, the SP2 (Droplet Measurement Technology, Inc., USA) was placed
114 after the DMA (Model 3081, TSI, USA) to measure the size-resolved BC mixing states,
115 and the instrument setup is schematically shown in Fig. S2. The DMA was set to scan
116 the aerosol over the size range between 12.3 and 697 nm every five minutes. The flow
117 rate leading to the SP2 and the condensation particle counter (CPC, Model 3776, TSI,
118 USA) were 0.12 and 0.28 L/min, respectively. The sheath flow of the DMA was 4 L/min.

119 The Aquadag was used to calibrate the measured incandescence signal of the SP2
120 using the DMA-SP2 system. The formula from Gysel et al. (2011) was used to convert
121 the mobility diameter into the mass of Aquadag. A correction factor of 0.75 was applied
122 to account for the different response sensitivity of SP2 to Aquadag and ambient BC
123 (Moteki et al., 2010).

In this study, the coating thickness of the BC-containing aerosols was calculated by the difference between the total mobility diameter measured by the DMA and the optical mass-equivalent diameters of the BC core ~~with the assumption that the density of the BC core is 1.8 g/cm³~~. Details of calculating the optical equivalent coating thickness can refer to Zhang et al. (2018b) and can be found in section 3 in the supplementary material.

2.2.2 Other instruments

The submicron particles (PM₁) chemical compositions were measured using a high-resolution time-of-flight aerosol mass spectrometer (AMS; Aerodyne Research Inc., Billerica, MA, USA). The data processing software PIKA (version 1.16) was used for data analysis. The positive matrix factorization (PMF) analysis was conducted for source appointment of the organic aerosols (Ulbrich et al., 2009). More details of the measurement of the aerosol chemical compositions and data processing can be found in Zheng et al. (2017).

The mass concentrations of O₃ were measured using UV absorption (model 49i, Thermo Fischer Inc. USA) with a time resolution of 1 minute. The mass concentrations of NO and NO₂ were measured using the chemiluminescence technique (NO-NO₂-NO_x Analyzer, Model 42i, Thermo Scientific, USA). The mass concentrations of SO₂ were measured using the ultraviolet fluorescence method (SO₂ analyzer, model 43i-TLE, Thermo Scientific, USA). The temperature (T), relative humidity (RH), wind speed (WS), and wind direction (WD) were monitored continuously during these campaigns.

2.3 Methodology

For the BC-containing aerosol, there is a lag between the peak time of the scattering and the incandescence signal (Metcalf et al., 2012). The lag time between the peak scattering signal and the peak incandescence signal can be employed to describe the

coating thickness (Moteki and Kondo, 2007; Schwarz et al., 2006) and further used to distinguish the BC-containing aerosols as ~~fresh~~-thinly and ~~aged~~-thickly coated ones. Despite that the time-lag method may not effectively distinguish the BC particles between fresh or aged ones because some BC particles sourced from biomass burning (Schwarz et al., 2008b) and solid fuel burning (Liu et al., 2014; Liu et al., 2019b) initially have a higher coating and were not aged ones. However, the lag-time probability distribution at our measurement sites show tow modes which will be shown in section 3.2 and thus the lag-time can be used to efficiently distinguish the BC-containign aerosols as thinly and thickly coated ones.

For the thickly coated BC particles, The-the measured scattering and incandescence signal can also be employed to distinguish the BC-containing particles as attached and coated types (Moteki et al., 2014) by calculating the time-dependent scattering cross-sections of BC-containing particles (Moteki and Kondo, 2007). For the coated type, all of the coating material will evaporate and the scattering cross-sections will decrease to zero after passing through the laser beam, while the scattering cross-section of the attached BC-containing aerosol will not decrease to zero (Moteki and Kondo, 2008). The method adopted by Dahlkötter et al. (2014) was employed here to characterize the morphology of the BC-containing aerosols. Details of distinguish the BC-contaning particles as attached and coated types can also refer to section 34 in the supplementary matials.

3 Results and discussions

3.1 Overview of the measurement results at different atmospheres

The time series of the measurement results are shown in Fig. S6, Fig. S7, and Fig. S8 for the PKU, CP, and LJ sites, respectively. ~~As f~~For the PKU site, the wind was mainly from the north and the wind speed was low with a mean value of 2.2 m/s. The

173 ambient atmosphere was very dry with a mean RH of 27.6%, with minimum and
174 maximum values of 5.8% and 72.6%, respectively. The temperature in the winter of
175 Beijing had a mean value of 0.8 °C between -5.9 °C and 9.2 °C. The mean mass
176 concentration of PM_{2.5} was 49.3 ± 55.4 µg/m³. The concentration of SO₂ and NO_x
177 (NO_x=NO + NO₂) had the same trends as PM_{2.5}, with mean values of 16.3±11.9 ppb
178 and 68.2±63.4 ppb, respectively. The O₃ concentration is anti-correlated with PM_{2.5}.
179 ~~The measurement site experienced four main pollution periods between 20, January and~~
180 ~~4, February, with each period lasting 2~4 days. The four pollution periods happened~~
181 ~~from 21 January to 24 January, from 24 January to 26 January, from 28 January to 29~~
182 ~~January, and from 31 January to 3 February. The PM_{2.5} peaked at the first pollution~~
183 ~~period, with 272.8 µg/m³. For each period, the high RH and low wind speed favored the~~
184 ~~development of pollution. At the end of each pollution period, the PM_{2.5} dropped~~
185 ~~dramatically with the increment of the wind speed and the change of the wind direction.~~
186 ~~The environment in the winter of Beijing was polluted, which was highly influenced by~~
187 ~~both primary particle emissions and secondary formation influenced by the meteorology~~
188 ~~conditions.~~ For the suburban site CP, the wind showed obvious diurnal cycles with high-
189 speed west wind during the day and low-speed east wind during the night. The mean
190 wind speed was 2.4±1.6 m/s. The RH during the campaign was 38.8±16.0%, with a
191 maximum value of 80.5%. The temperature during the campaign was 21.8±5.2 °C with
192 a maximum value of 33.2 °C. As for the NO_x, the mean concentration was 21.4±17.7
193 ppb. ~~The concentration of NO_x experienced high value during the early morning, and~~
194 ~~fluctuated dramatically, which is highly related to the anthropogenic activities.~~ The
195 mean concentration of SO₂ was 2.89±1.10 ppb. ~~The measured SO₂ concentration values~~
196 ~~during the day were higher than those at night. There was no obvious diurnal cycle for~~

~~the SO₂ concentration, and dramatic fluctuation was not observed, which indicates that the SO₂ was mainly from transportation.~~ The measured mean O₃ concentration was 54.5 ± 38.8 ppb. The mean PM_{2.5} concentration was 22.6 ± 16.8 µg/m³, with a maximum value of 71.8 µg/m³. As for the background LJ site, The mean value of the wind speed, RH, and T were 3.13 m/s, 50.23%, and 6.5 °C, respectively. The mean PM_{2.5} mass concentration was 6.2 ± 5.7 µg/m³. The mean NO_x and SO₂ concentrations were 0.05 ppb and 0.97 ppb respectively.

The characteristics of the measurement sites are summarized and shown in Fig. 1. The differences in the temperature and RH among these sites were mainly resulted from the that the measurements were conducted in different seasons. The concentrations of SO₂, NO_x, and PM_{2.5} indicated that the urban site PKU was most polluted. The suburban site CP was slightly polluted and the background LJ was the cleanest.

The air mass back trajectories as shown in Fig. S9 during the measurement at PKU show that the measurement site was mainly influenced by the polluted air from south and southeast, and the relative clean air from northwest. The CP site was mainly influenced by the clean air from the northwest and the polluted air from southeast. The air mass of LJ site was mainly from the southwest and west.

3.2 Mixing states of the ~~fresh~~ thinly coated and ~~aged~~ thickly coated BC-containing aerosols

The measured lag time probability distributions for the PKU, CP and LJ sites are shown in Fig. 2 (a), (b), and (c), respectively. The lag time had two modes for each measurement site. Therefore, the BC particles are sorted as thinly or thickly coated BC. – A two log-normal distribution was used for the probability distribution of the lag time for BC-containing particles as:

$$\text{PDF}(\Delta t) = \sum_{i=1,2} \frac{A_i}{\sqrt{2\pi} \log(\sigma_{g,i})} \exp \left[-\frac{\log(\Delta t) - \log(\Delta t_i)}{2 \log^2(\sigma_{g,i})} \right]^2$$

Where Δt is the lag time, A_i , $\sigma_{g,i}$, Δt_i are the scale factor, geometric standard deviation, and geometric mean lag time of mode i respectively. The critical lag time that distinguish the thinly and thickly BC particles was determined by calculating the value when the probability distribution values of mode 1 and mode 2 are equal. In this study, the BC-containing aerosols with a lag time larger than 1.4 μs were classified as ~~aged~~ thickly coated particles for LJ site. The other BC-containing aerosols were classified as ~~fresh~~ thinly coated particles. Our critical lag time of 1.4 μs is smaller than the previous studies that distinguished the BC-containing aerosols between ~~fresh~~ thinly coated BC and ~~aged~~ thickly coated BC with a lag time of 2 μs (Moteki and Kondo, 2007; Metcalf et al., 2012) ~~or~~ 1.8 μs (Metcalf et al., 2012), and 4.2 μs (Liu et al., 2010), which was determined by the internal setup up of the SP2. The critical lag time for the PKU and CP sites were 1.3 μs and 1.7 μs , respectively.

For each type of BC-containing aerosols, we calculated the coating thickness probabilities and the results are shown in Fig. 2(d), (e) and (f) for the PKU, CP, and LJ sites, respectively. Results showed that the BC-containing aerosols were mainly composed of thickly coated ~~aged~~ BC aerosols and thinly coated ~~fresh~~ BC aerosols. The coating thickness for the ~~fresh~~ thinly coated BC-containing aerosol was smaller than that of the ~~aged~~ thickly coated BC-containing aerosols. However, the coating thickness of the ~~aged~~ thickly coated BC-containing aerosols spread wider than that of the ~~fresh~~ thinly coated ones.

The number fractions of the ~~aged~~ thickly coated BC-containing aerosols were significantly different for different atmospheres as shown in Fig. 2 (g), (h), and (i). At

the polluted urban site, the number concentration of the aged thickly coated BC-containing aerosols was comparable to that of the fresh thinly coated BC-containing aerosols with the number fractions of 561% and 4944% for the fresh thinly coated and aged thickly coated BC particles, respectively. The number fraction of the aged thickly coated BC aerosols at the CP site was 67 %. However, the BC-containing aerosols at the background LJ site were dominated by aged thickly coated ones with a number fraction of 7981%.

The difference in the number fraction of the aged thickly coated BC particles was synthetically influenced by the ambient pollution levels and the sources of the BC aerosols. The suburban site CP had the largest number fraction of the fresh thinly coated BC particles. The CP site is not far from the urban, and thus the fresh thinly coated BC particles from the traffic contribute a large amount of the total ones. The urban site PKU had a larger number fraction of the aged thickly coated BC than that of the CP site. This might be resulted from that the PKU site being more polluted than the CP site and then the aging processing at the PKU site was faster than that at the CP site. The LJ site is far from the traffic sources. The measured BC particles at the LJ site were mainly from long-range transportation and experienced a long time of aging process than that at the CP and PKU sites. Therefore, the BC-containing aerosols were dominated by the aged thickly coated ones at the LJ sites.

We compared the number fraction of the aged thickly coated BC at different measurement sites from literature (Ueda et al., 2016; Schwarz et al., 2008a; Wang et al., 2017c; Wang et al., 2017a; Wu et al., 2017; Wang et al., 2017b; Wang et al., 2014; Huang et al., 2012; Metcalf et al., 2012; Wang et al., 2016; Shiraiwa et al., 2007; Mcmeeking et al., 2012; Subramanian et al., 2010; Schwarz et al., 2008b; Saha et al., 2018; Krasowsky et al., 2018; Holder et al., 2014) and the results are shown in Fig. 3. The number fraction values were divided into three different kinds of groups, namely

the roadside, urban or suburban, and background. Results from Fig. 3 show that the number fractions at the roadside tend to be the lowest. These sites were close to the traffic sources and the measured BC-containing aerosols were mainly from the traffic. The left part of the green circles correspond to the relatively clean urban or suburban sites with the number fractions of the aged thickly coated BC around 30%. However, the number fractions of the relative polluted urban or suburban sites had a larger number fraction of the aged thickly coated BC around 50%. The number fractions of the aged thickly coated BC at the background sites were the largest. Therefore, the number fractions of the aged thickly coated BC-containing aerosols were synthetically influenced by the distance from the primary source and the pollution levels of the ambient atmosphere. The number fraction of the aged thickly coated BC-containing aerosols increased with the distance from the primary emission sources and the pollution levels. Our results were consistent with the aerial measurement by Metcalf et al. (2012), who found that the number fraction of the aged thickly coated BC was 29%~41% at the top of the Los Angeles city and 47%-54% for the out plume of this city.

For a better understanding of the source of the fresh thinly coated and aged thickly coated BC, we compared the number concentrations of the BC-containing aerosols with the source apportionment results from the AMS data for the CP site. Among the PMF results, the factor of hydrocarbon-like organic aerosol (HOA) is mainly composed of long-chain hydrocarbon, and oxygenated organic aerosol (OOA) is mainly from the secondary formation. HOA is mainly from the diesel exhaust, gasoline exhaust, and lubricating oil emission. From Fig. 4(a), the number concentration of the fresh thinly coated BC and mass concentration of HOA showed good consistency, with R^2 equaling 0.69 as shown in Fig. S10, which further proved the evidence that the fresh thinly coated BC-containing aerosols were from the traffic sources. The time series of the aged thickly coated BC and OOA showed good consistency as shown in Fig. 4 (b), with R^2 equaling

0.87. Therefore, the aging processing of the ambient BC was accompanied by the ambient OA. The mass concentration of OOA and number concentration of aged thickly coated BC can be used as good indicators for each other.

3.3 Size distributions of the fresh thinly coated and aged thickly coated BC-containing aerosols

The size distributions of the BC-containing aerosols exert significant influence on their corresponding radiative effects (Zhao et al., 2019; Matsui et al., 2018). We calculated the number size distribution (NSD) of BC-containing aerosols for the fresh thinly coated and aged thickly coated ones at different sites, and the results are shown in Fig. 5. It should be noted that the D_p in Fig. 5 corresponds to the mobility diameter from the DMA. The BC-containing aerosol NSD was further fit using the log-normal distribution.

As for the fresh thinly coated BC-containing aerosols, the geometric mean diameters ($\overline{D_m}$) were 193, 161, and 162 nm for the PKU, CP, and LJ sites, respectively. The geometric standard deviations (GSD) of the BC-containing aerosol NSD were 1.50, 1.63, 1.91 for the PKU, CP, and LJ sites, respectively. The GSD to some extent reflects the diversity of the BC sources. The LJ site had the largest GSD, which indicated multiple sources of fresh thinly coated BC-containing aerosols. The LJ site was highly influenced by atmospheric transportation, due to the high altitude of this location (Zheng et al., 2017; Tan et al., 2021). Therefore, the fresh thinly coated BC-containing aerosols could be originated from different orientations. As for the urban site PKU, the fresh thinly coated BC aerosols were mainly from urban lifestyle emissions. Therefore, the fresh thinly coated BC aerosols at the PKU site had the lowest value of the GSD. However, the fresh thinly coated BC aerosols at the suburban site CP were influenced synthetically

by urban lifestyle sources and some other sources from suburban, and thus had a larger value of GSD than that of PKU.

As for the aged thickly coated BC, it is obvious that they had larger diameters than those of the fresh thinly coated BC due to the coating of other non-BC components. The geometric mean D_p/D_m values of the aged thickly coated BC were 294, 244, and 257 nm for the PKU, CP, and LJ sites, respectively. The corresponding GSD values were 1.37, 1.41, and 1.46.

Based on the above results, the geometric mean D_p/D_m values of the aged thickly coated BC aerosols were larger than that of the fresh thinly coated BC aerosols by 52%, 52%, and 59% for the PKU, CP, and LJ sites, respectively. The GSD values of the aged thickly coated BC were consistent with that of the fresh thinly coated BC with the lowest value at the PKU site and highest value at the LJ site, which is consistent with the diversity of the sources of BC-containing aerosols. For each site, the GSD values of the aged thickly coated BC aerosols were smaller than that of the fresh thinly coated ones. The GSD of BC-containing aerosols tend to be smaller during the aging processing because the increment of the diameter should decrease with the diameter.

3.4 Size distribution of the fresh thinly coated and aged thickly coated BC core

The number and mass concentrations of the BC core under different mass equivalent diameters were calculated ~~with the assumption that the BC core has an effective density of 1.8 g/cm^3~~ and the results are shown in Fig. 6 and Table 1. It should be noted here that, when it comes to the BC size distribution, the mass-equivalent diameter of BC cores (D_{me}) (assuming a density of 1.8 g/cm^3) was adopted in this study for direct comparison with previous studies. From Fig. 6

As for the number size distribution of the BC core, the geometric mean D_{me} mass equivalent diameter (D_{me}) of the fresh thinly coated BC particles were 115, 107, and 127 nm, for the PKU, CP, and LJ sites respectively. The corresponding GSD values are 1.58 1.53 and 1.68, respectively. The D_{me} for the aged thickly coated BC particles were 114, 95, and 111 nm for the PKU, CP, and LJ sites respectively and the corresponding GSD values were 1.40, 1.45, and 1.43, respectively. Both the GSD and the D_{me} of the aged thickly coated BC were smaller than that of the fresh thinly coated BC. ~~This might be resulted from the fact that the small BC particles have a longer life than that of the large BC particles.~~ The overall geometric mean diameter of the BC core number size distributions are 114, 100, and 111 nm for the PKU, CP and LJ sites respectively.

There are mainly two-three possible reasons that may lead to the smaller geometric mean diameter for the thinly coated BC than the thickly coated BC. First, the smaller BC core tend to have higher time-lag as a smaller BC core will take a longer time to evaporate the coating on it and thus the thinly coated particles tend to have smaller core diameters. Second, it takes less time for the smaller BC particles to grow the same amount of coating thickness when the increment of the BC particles were dominated by condensation. ~~This might be resulted from the fact that~~ Thirdly, the small BC particles may have a longer life than that of the large BC particles..

As for the mass size distribution of the BC core, the geometric mean D_{me} of the thinly coated BC were 187, 182, 238 nm for the PKU, CP and LJ sites respectively and the corresponding GSD values were 1.35, 1.48, 1.47. The overall geometric mean diameter of the BC core mass distributions are 172, 169, 181 nm for the PKU, CP and LJ sites respectively. The geometric mean diameter of the BC core mass distributions

of 172 nm in PKU were slightly smaller than that from Liu et al. (2019a), with geometric mean diameter of 195 nm in another measurement in urban environment in Beijing and comparable to the of Zhang et al. (2018a) with geometric mean diameter of the BC core around 180 nm.

3.5 Morphology of the BC-containing aerosols

The time series of the number fractions of the attached BC-containing aerosols to the total BC-containing aerosols (f_{attached}) are shown in Fig. 7. From Fig. 7, the f_{attached} ranged between 0 and 0.21 with a mean value of $7.2 \pm 3.7\%$, $11.0 \pm 3.7\%$, and $10.1 \pm 4.1\%$. Moteki et al. (2014) found that the f_{attached} was generally less than 0.1 in Tokyo. The f_{attached} ranged between 3% and 16% in suburban London (Liu et al., 2015). A mean value of 12% was found for biomass burning particles using electron microscopy (China et al., 2013). Our measurement results were consistent with the previous studies. The f_{attached} tend to increase with the $\text{PM}_{2.5}$ for different sites, which may indicate that the attached BC-containing aerosols were generated from the coagulation of BC and non-BC aerosols.

We calculated the f_{attached} under different aerosol diameters and the results are shown in Fig. 8. There were few attached BC-containing aerosols when the diameter was smaller than 250 nm with f_{attached} lower than 2%. The f_{attached} increased with the diameter for all of the measurement sites. It could reach 30% for the LJ sites. Based on the results from the electron microscopy, the BC volume fractions are smaller than those of the non-BC volume fractions in the attached BC aerosols (Moteki et al., 2014). The increment of f_{attached} with D_p is essentially consistent with the results from Hu et al. (2021a) that larger D_p contains more fractal BC, which is hard to be enveloped by coatings. Our results further indicate that the attached BC aerosols were formed from coagulation, as the coagulation efficiency of the two particles increased with the

392 difference between their sizes (Cai and Jiang, 2017; Kim et al., 2016; Mahfouz and
393 Donahue, 2021).

394 Under the heavier pollution, more secondary aerosol forms and more condensation
395 process would on one hand increase the coating of the previous coated BC particles,
396 which would not increase the number fraction of coated BC. On the other hand, the
397 condensation process would coating on the attached BC particle and to some content
398 would lead to transformation from the attached BC to coated BC particles. Based on our
399 measurement results, the above process of transform from attached BC to coated BC
400 may not comparable to the process of coagulation between thinly coated BC and non-
401 BC particles, which would lead to the increament of the fraction of attached BC with
402 the pollution levels.

403 The f_{attached} under different aerosol number concentrations (N) and different ratios of
404 the BC-free aerosol number concentrations to the BC-containing aerosol number
405 concentrations are shown in Fig. 9. Results showed that the f_{attached} increased with the
406 above two factors. The results were consistent with the fact that the coagulation between
407 BC and non-BC components is more likely to happen with the increment of the BC-free
408 aerosol number concentrations. Based on the analysis above, we concluded that the
409 attached BC- containing aerosols are mainly formed through coagulation.

410 4 Conclusions

411 In this study, the BC microphysical properties were studied based on field
412 measurement using the DMA-SP2 system at the urban site PKU, suburban site CP and
413 a background site LJ in China.

414 ~~The BC-containing aerosols were sorted as aged thickly coated BC and fresh thinly~~
415 ~~coated BC based on the lag time between the peak position of the light scattering signals~~

~~and the incandescence signals.~~ The number fractions of the aged thickly coated BC-containing aerosols were 49%, 33%, and 79% for the PKU, CP, and LJ sites respectively. The mass concentrations of the fresh thinly coated BC-containing aerosols showed good consistency with that of HOA, which indicated that the fresh thinly coated BC-containing aerosols were mainly generated from the emission of vehicles. The aged thickly coated BC-containing aerosols are highly correlated with the OOA.

The geometric diameter of the fresh thinly coated BC-containing aerosols ranged between 160 nm and 200 nm, while the corresponding range was 240~300 nm for the aged thickly coated BC-containing aerosols. The GSD of the BC-containing aerosols decreased during the aging process. The corresponding mobility diameters of these aged thickly coated (fresh thinly coated) BC-containing aerosols were 294 (193), 244 (161), and 257 (162) nm. The measured aged thickly coated (fresh thinly coated) BC core number median diameters were 115 (114), 107 (95), and 127 (111) nm for the urban, suburban, and background sites, respectively. The corresponding aged thickly coated (fresh thinly coated) core mass median diameters were 187 (154), 182 (146), and 238 (163) nm respectively. The mean diameter of the aged thickly coated BC-containing aerosols was larger than that of the fresh thinly coated BC-containing aerosols, while the mean BC core diameter of the aged thickly coated BC-containing aerosols was smaller than that of the fresh thinly coated BC-containing aerosols. ~~The BC-containing aerosols were sorted as the coated type when the scattering cross-section decreased to zeros, while the BC-containing aerosols were sorted as the attached type when the scattering cross-section was still larger than a critical point after passing through the SP2 laser beam.~~ There are about 10% of the BC-containing aerosols with the BC core attached to the other non-BC components. We concluded that these se attached BC-containing aerosols were mainly generated by coagulation between the BC and non-BC

components despite the fact that the aging of the ambient BC aerosols were driven by condensation.

Data availability. The data is available at <https://doi.org/10.5281/zenodo.5816310>.

Author contributions. **Gang Zhao:** Conceptualization, Writing - Original Draft, Visualization, Software, **Tianyi Tan:** Data Curation, Conceptualization, Visualization, **Shuya Hu:** Data Curation, Conceptualization, **Zhuofei Du:** Data Curation, **Dongjie Shang:** Data Curation, **Zhijun Wu:** Data Curation, Conceptualization, **Song Guo:** Data Curation, Conceptualization, **Jing Zheng:** Data Curation, Conceptualization, **Wenfei Zhu:** Data Curation, Conceptualization, **Mengren Li:** Data Curation, Conceptualization, **Limin Zeng:** Data Curation, Conceptualization, **Min Hu:** Resources, Supervision, Data Curation, Conceptualization, Revision.

Competing interests. The authors declare that they have no conflict of interest.

Acknowledgments. This work is supported by the China Postdoctoral Science Foundation (2021M700192) and National Natural Science Foundation of China (91844301).

References

- Bond, T. C. and Bergstrom, R. W.: Light Absorption by Carbonaceous Particles: An Investigative Review, *Aerosol Sci. Technol.*, 40, 27-67, 10.1080/02786820500421521, 2006.
- Bond, T. C., Doherty, S. J., Fahey, D. W., Forster, P. M., Berntsen, T., DeAngelo, B. J., Flanner, M. G., Ghan, S., Karcher, B., Koch, D., Kinne, S., Kondo, Y., Quinn, P. K., Sarofim, M. C., Schultz, M. G., Schulz, M., Venkataraman, C., Zhang, H., Zhang, S.,

464 Bellouin, N., Guttikunda, S. K., Hopke, P. K., Jacobson, M. Z., Kaiser, J. W., Klimont,
 465 Z., Lohmann, U., Schwarz, J. P., Shindell, D., Storelvmo, T., Warren, S. G., and Zender,
 466 C. S.: Bounding the role of black carbon in the climate system: A scientific assessment,
 467 *J Geophys Res-Atmos*, 118, 5380-5552, 10.1002/jgrd.50171, 2013.

468 Cai, R. and Jiang, J.: A new balance formula to estimate new particle formation rate:
 469 reevaluating the effect of coagulation scavenging, *Atmospheric Chemistry and Physics*,
 470 17, 12659-12675, 10.5194/acp-17-12659-2017, 2017.

471 China, S., Mazzoleni, C., Gorkowski, K., Aiken, A. C., and Dubey, M. K.: Morphology
 472 and mixing state of individual freshly emitted wildfire carbonaceous particles, *Nature*
 473 *communications*, 4, 2122, 10.1038/ncomms3122, 2013.

474 Dahlkötter, F., Gysel, M., Sauer, D., Minikin, A., Baumann, R., Seifert, P., Ansmann,
 475 A., Fromm, M., Voigt, C., and Weinzierl, B.: The Pagami Creek smoke plume after
 476 long-range transport to the upper troposphere over Europe – aerosol properties
 477 and black carbon mixing state, *Atmospheric Chemistry and Physics*, 14, 6111-6137,
 478 10.5194/acp-14-6111-2014, 2014.

479 Ding, A., Huang, X., Nie, W., Sun, J., Kerminen, V.-M., Petäjä T., Su, H., Cheng, Y.,
 480 Yang, X.-Q., Wang, M., Chi, X., Wang, J., Virkkula, A., Guo, W., Yuan, J., Wang, S.
 481 R., Zhang, R., Wu, Y., Song, Y. C., Zhu, T., Zilitinkevich, S., Kulmala, M., and Fu, C.:
 482 Enhanced haze pollution by black carbon in megacities in China, *Geophys. Res. Lett.*,
 483 43, 2873-2879, 2016.

484 Ding, S., Liu, D., Zhao, D., Hu, K., Tian, P., Zhou, W., Huang, M., Yang, Y., Wang, F.,
 485 Sheng, J., Liu, Q., Kong, S., Cui, P., Huang, Y., He, H., Coe, H., and Ding, D.: Size-
 486 Related Physical Properties of Black Carbon in the Lower Atmosphere over Beijing and
 487 Europe, *Environ Sci Technol*, 53, 11112-11121, 10.1021/acs.est.9b03722, 2019.

488 Gysel, M., Laborde, M., Olfert, J. S., Subramanian, R., and Gröhn, A. J.: Effective
 489 density of Aquadag and fullerene soot black carbon reference materials used for SP2

calibration, *Atmospheric Measurement Techniques*, 4, 2851-2858, 10.5194/amt-4-2851-2011, 2011.

Holder, A. L., Hagler, G. S. W., Yelverton, T. L. B., and Hays, M. D.: On-road black carbon instrument intercomparison and aerosol characteristics by driving environment, *Atmospheric Environment*, 88, 183-191, <https://doi.org/10.1016/j.atmosenv.2014.01.021>, 2014.

Hu, K., Liu, D., Tian, P., Wu, Y., Deng, Z., Wu, Y., Zhao, D., Li, R., Sheng, J., Huang, M., Ding, D., Li, W., Wang, Y., and Wu, Y.: Measurements of the Diversity of Shape and Mixing State for Ambient Black Carbon Particles, *Geophys. Res. Lett.*, 48, 10.1029/2021gl094522, 2021a.

Hu, S., Zhao, G., Tan, T., Li, C., Zong, T., Xu, N., Zhu, W., and Hu, M.: Current challenges of improving visibility due to increasing nitrate fraction in PM_{2.5} during the haze days in Beijing, China, *Environmental Pollution*, 290, 118032, 10.1016/j.envpol.2021.118032, 2021b.

Hu, W., Hu, M., Hu, W.-W., Zheng, J., Chen, C., Wu, Y., and Guo, S.: Seasonal variations in high time-resolved chemical compositions, sources, and evolution of atmospheric submicron aerosols in the megacity Beijing, *Atmospheric Chemistry and Physics*, 17, 9979-10000, 10.5194/acp-17-9979-2017, 2017.

Huang, X.-F., Sun, T.-L., Zeng, L.-W., Yu, G.-H., and Luan, S.-J.: Black carbon aerosol characterization in a coastal city in South China using a single particle soot photometer, *Atmospheric Environment*, 51, 21-28, <https://doi.org/10.1016/j.atmosenv.2012.01.056>, 2012.

Kim, Y.-h., Yiacoumi, S., Nenes, A., and Tsouris, C.: Charging and coagulation of radioactive and nonradioactive particles in the atmosphere, *Atmospheric Chemistry and Physics*, 16, 3449-3462, 10.5194/acp-16-3449-2016, 2016.

Krasowsky, T. S., McMeeking, G. R., Sioutas, C., and Ban-Weiss, G.: Characterizing the evolution of physical properties and mixing state of black carbon particles: from

517 near a major highway to the broader urban plume in Los Angeles, *Atmos. Chem. Phys.*,
 518 18, 11991-12010, 10.5194/acp-18-11991-2018, 2018.

519 Liu, D., Allan, J. D., Young, D. E., Coe, H., Beddows, D., Fleming, Z. L., Flynn, M. J.,
 520 Gallagher, M. W., Harrison, R. M., Lee, J., Prevot, A. S. H., Taylor, J. W., Yin, J.,
 521 Williams, P. I., and Zotter, P.: Size distribution, mixing state and source apportionment
 522 of black carbon aerosol in London during wintertime, *Atmospheric Chemistry and*
 523 *Physics*, 14, 10061-10084, 10.5194/acp-14-10061-2014, 2014.

524 Liu, D., Joshi, R., Wang, J., Yu, C., Allan, J. D., Coe, H., Flynn, M. J., Xie, C., Lee, J.,
 525 Squires, F., Kotthaus, S., Grimmond, S., Ge, X., Sun, Y., and Fu, P.: Contrasting
 526 physical properties of black carbon in urban Beijing between winter and summer,
 527 *Atmospheric Chemistry and Physics*, 19, 6749-6769, 10.5194/acp-19-6749-2019,
 528 2019a.

529 Liu, D., Flynn, M., Gysel, M., Targino, A., Crawford, I., Bower, K., Choularton, T.,
 530 Jurányi, Z., Steinbacher, M., Hüglin, C., Curtius, J., Kampus, M., Petzold, A.,
 531 Weingartner, E., Baltensperger, U., and Coe, H.: Single particle characterization of
 532 black carbon aerosols at a tropospheric alpine site in Switzerland, *Atmospheric*
 533 *Chemistry and Physics*, 10, 7389-7407, 10.5194/acp-10-7389-2010, 2010.

534 Liu, H., Pan, X., Liu, D., Liu, X., Chen, X., Tian, Y., Sun, Y., Fu, P., and Wang, Z.:
 535 Mixing characteristics of refractory black carbon aerosols determined by a tandem
 536 CPMA-SP2 system at an urban site in Beijing, *Atmospheric Chemistry and Physics*
 537 *Discussions*, 1-25, 10.5194/acp-2019-244, 2019b.

538 Liu, S., Aiken, A. C., Gorkowski, K., Dubey, M. K., Cappa, C. D., Williams, L. R.,
 539 Herndon, S. C., Massoli, P., Fortner, E. C., Chhabra, P. S., Brooks, W. A., Onasch, T.
 540 B., Jayne, J. T., Worsnop, D. R., China, S., Sharma, N., Mazzoleni, C., Xu, L., Ng, N.
 541 L., Liu, D., Allan, J. D., Lee, J. D., Fleming, Z. L., Mohr, C., Zotter, P., Szidat, S., and
 542 Prevot, A. S.: Enhanced light absorption by mixed source black and brown carbon
 543 particles in UK winter, *Nature communications*, 6, 8435, 10.1038/ncomms9435, 2015.

544 Mahfouz, N. G. A. and Donahue, N. M.: Technical note: The enhancement limit of
 545 coagulation scavenging of small charged particles, *Atmos. Chem. Phys.*, 21, 3827-3832,
 546 10.5194/acp-21-3827-2021, 2021.

547 Matsui, H., Hamilton, D. S., and Mahowald, N. M.: Black carbon radiative effects
 548 highly sensitive to emitted particle size when resolving mixing-state diversity, *Nature*
 549 *communications*, 9, 3446, 10.1038/s41467-018-05635-1, 2018.

550 McMeeking, G. R., Bart, M., Chazette, P., Haywood, J. M., Hopkins, J. R., McQuaid,
 551 J. B., Morgan, W. T., Raut, J. C., Ryder, C. L., Savage, N., Turnbull, K., and Coe, H.:
 552 Airborne measurements of trace gases and aerosols over the London metropolitan region,
 553 *Atmos. Chem. Phys.*, 12, 5163-5187, 10.5194/acp-12-5163-2012, 2012.

554 Menon, S., Hansen, J., Nazarenko, L., and Luo, Y.: Climate effects of black carbon
 555 aerosols in China and India, *Science*, 297, 2250-2253, 10.1126/science.1075159, 2002.

556 Metcalf, A. R., Craven, J. S., Ensberg, J. J., Brioude, J., Angevine, W., Sorooshian, A.,
 557 Duong, H. T., Jonsson, H. H., Flagan, R. C., and Seinfeld, J. H.: Black carbon aerosol
 558 over the Los Angeles Basin during CalNex, *Journal of Geophysical Research:*
 559 *Atmospheres*, 117, <https://doi.org/10.1029/2011JD017255>, 2012.

560 Moffet, R. C., amp, apos, Brien, R. E., Alpert, P. A., Kelly, S. T., Pham, D. Q., Gilles,
 561 M. K., Knopf, D. A., and Laskin, A.: Morphology and mixing of black carbon particles
 562 collected in central California during the CARES field study, *Atmospheric Chemistry*
 563 *and Physics*, 16, 14515-14525, 10.5194/acp-16-14515-2016, 2016.

564 Moteki, N. and Kondo, Y.: Effects of Mixing State on Black Carbon Measurements by
 565 Laser-Induced Incandescence, *Aerosol Sci. Technol.*, 41, 398-417,
 566 10.1080/02786820701199728, 2007.

567 Moteki, N. and Kondo, Y.: Method to measure time-dependent scattering cross sections
 568 of particles evaporating in a laser beam, *Journal of Aerosol Science*, 39, 348-364,
 569 10.1016/j.jaerosci.2007.12.002, 2008.

570 Moteki, N. and Kondo, Y.: Dependence of Laser-Induced Incandescence on Physical
 571 Properties of Black Carbon Aerosols: Measurements and Theoretical Interpretation,
 572 Aerosol Sci. Technol., 44, 663-675, Pii 924375405
 573 10.1080/02786826.2010.484450, 2010.
 574 Moteki, N., Kondo, Y., and Adachi, K.: Identification by single-particle soot photometer
 575 of black carbon particles attached to other particles: Laboratory experiments and ground
 576 observations in Tokyo, Journal of Geophysical Research: Atmospheres, 119, 1031-1043,
 577 <https://doi.org/10.1002/2013JD020655>, 2014.
 578 Moteki, N., Kondo, Y., and Nakamura, S.-i.: Method to measure refractive indices of
 579 small nonspherical particles: Application to black carbon particles, Journal of Aerosol
 580 Science, 41, 513-521, <https://doi.org/10.1016/j.jaerosci.2010.02.013>, 2010.
 581 Peng, J., Hu, M., Guo, S., Du, Z., Zheng, J., Shang, D., Levy Zamora, M., Zeng, L.,
 582 Shao, M., Wu, Y.-S., Zheng, J., Wang, Y., Glen, C. R., Collins, D. R., Molina, M. J.,
 583 and Zhang, R.: Markedly enhanced absorption and direct radiative forcing of black
 584 carbon under polluted urban environments, Proceedings of the National Academy of
 585 Sciences, 201602310, 10.1073/pnas.1602310113, 2016.
 586 Ramanathan, V. and Carmichael, G.: Global and regional climate changes due to black
 587 carbon, Nature Geoscience, 1, 221-227, 10.1038/ngeo156, 2008.
 588 Roberts, G. C., Ramana, M. V., Corrigan, C., Kim, D., and Ramanathan, V.:
 589 Simultaneous observations of aerosol-cloud-albedo interactions with three stacked
 590 unmanned aerial vehicles, Proceedings of the National Academy of Sciences of the
 591 United States of America, 105, 7370-7375, 10.1073/pnas.0710308105, 2008.
 592 Saha, P. K., Khlystov, A., and Grieshop, A. P.: Downwind evolution of the volatility
 593 and mixing state of near-road aerosols near a US interstate highway, Atmos. Chem.
 594 Phys., 18, 2139-2154, 10.5194/acp-18-2139-2018, 2018.

595 Schwarz, J. P., Spackman, J. R., Fahey, D. W., Gao, R. S., Lohmann, U., Stier, P., Watts,
 596 L. A., Thomson, D. S., Lack, D. A., Pfister, L., Mahoney, M. J., Baumgardner, D.,
 597 Wilson, J. C., and Reeves, J. M.: Coatings and their enhancement of black carbon light
 598 absorption in the tropical atmosphere, *J Geophys Res-Atmos*, 113,
 599 10.1029/2007jd009042, 2008a.

600 Schwarz, J. P., Gao, R. S., Spackman, J. R., Watts, L. A., Thomson, D. S., Fahey, D.
 601 W., Ryerson, T. B., Peischl, J., Holloway, J. S., Trainer, M., Frost, G. J., Baynard, T.,
 602 Lack, D. A., de Gouw, J. A., Warneke, C., and Del Negro, L. A.: Measurement of the
 603 mixing state, mass, and optical size of individual black carbon particles in urban and
 604 biomass burning emissions, *Geophys. Res. Lett.*, 35,
 605 <https://doi.org/10.1029/2008GL033968>, 2008b.

606 Schwarz, J. P., Gao, R. S., Fahey, D. W., Thomson, D. S., Watts, L. A., Wilson, J. C.,
 607 Reeves, J. M., Darbeheshti, M., Baumgardner, D. G., Kok, G. L., Chung, S. H., Schulz,
 608 M., Hendricks, J., Lauer, A., Kärcher, B., Slowik, J. G., Rosenlof, K. H., Thompson, T.
 609 L., Langford, A. O., Loewenstein, M., and Aikin, K. C.: Single-particle measurements
 610 of midlatitude black carbon and light-scattering aerosols from the boundary layer to the
 611 lower stratosphere, *Journal of Geophysical Research*, 111, 10.1029/2006jd007076,
 612 2006.

613 Shang, D., Hu, M., Zheng, J., Qin, Y., Du, Z., Li, M., Fang, J., Peng, J., Wu, Y., Lu, S.,
 614 and Guo, S.: Particle number size distribution and new particle formation under the
 615 influence of biomass burning at a high altitude background site at Mt. Yulong (3410 m),
 616 China, *Atmospheric Chemistry and Physics*, 18, 15687-15703, 10.5194/acp-18-15687-
 617 2018, 2018.

618 Shiraiwa, M., Kondo, Y., Moteki, N., Takegawa, N., Miyazaki, Y., and Blake, D. R.:
 619 Evolution of mixing state of black carbon in polluted air from Tokyo, *Geophys. Res.*
 620 *Lett.*, 34, <https://doi.org/10.1029/2007GL029819>, 2007.

621 Subramanian, R., Kok, G. L., Baumgardner, D., Clarke, A., Shinozuka, Y., Campos, T.
 622 L., Heizer, C. G., Stephens, B. B., de Foy, B., Voss, P. B., and Zaveri, R. A.: Black
 623 carbon over Mexico: the effect of atmospheric transport on mixing state, mass
 624 absorption cross-section, and BC/CO ratios, *Atmos. Chem. Phys.*, 10, 219-237,
 625 10.5194/acp-10-219-2010, 2010.

626 Tan, T., Hu, M., Du, Z., Zhao, G., Shang, D., Zheng, J., Qin, Y., Li, M., Wu, Y., Zeng,
 627 L., Guo, S., and Wu, Z.: Measurement report: Strong light absorption induced by aged
 628 biomass burning black carbon over the southeastern Tibetan Plateau in pre-monsoon
 629 season, *Atmospheric Chemistry and Physics*, 21, 8499-8510, 10.5194/acp-21-8499-
 630 2021, 2021.

631 Ueda, S., Nakayama, T., Taketani, F., Adachi, K., Matsuki, A., Iwamoto, Y., Sadanaga,
 632 Y., and Matsumi, Y.: Light absorption and morphological properties of soot-containing
 633 aerosols observed at an East Asian outflow site, Noto Peninsula, Japan, *Atmos. Chem.*
 634 *Phys.*, 16, 2525-2541, 10.5194/acp-16-2525-2016, 2016.

635 Ulbrich, I. M., Canagaratna, M. R., Zhang, Q., Worsnop, D. R., and Jimenez, J. L.:
 636 Interpretation of organic components from Positive Matrix Factorization of aerosol
 637 mass spectrometric data, *Atmospheric Chemistry and Physics*, 9, 2891-2918,
 638 10.5194/acp-9-2891-2009, 2009.

639 Wang, J., Zhang, Q., Chen, M., Collier, S., Zhou, S., Ge, X., Xu, J., Shi, J., Xie, C., Hu,
 640 J., Ge, S., Sun, Y., and Coe, H.: First Chemical Characterization of Refractory Black
 641 Carbon Aerosols and Associated Coatings over the Tibetan Plateau (4730 m a.s.l),
 642 *Environmental Science & Technology*, 51, 14072-14082, 10.1021/acs.est.7b03973,
 643 2017a.

644 Wang, Q., Huang, R. J., Cao, J., Han, Y., Wang, G., Li, G., Wang, Y., Dai, W., Zhang,
 645 R., and Zhou, Y.: Mixing State of Black Carbon Aerosol in a Heavily Polluted Urban
 646 Area of China: Implications for Light Absorption Enhancement, *Aerosol Sci. Technol.*,
 647 48, 689-697, 10.1080/02786826.2014.917758, 2014.

648 Wang, Q., Huang, R., Zhao, Z., Cao, J., Ni, H., Tie, X., Zhu, C., Shen, Z., Wang, M.,
 649 Dai, W., Han, Y., Zhang, N., and Prevot, A. S. H.: Effects of photochemical oxidation
 650 on the mixing state and light absorption of black carbon in the urban atmosphere of
 651 China, *Environmental Research Letters*, 12, 10.1088/1748-9326/aa64ea, 2017b.
 652 Wang, Q., Huang, R.-J., Zhao, Z., Zhang, N., Wang, Y., Ni, H., Tie, X., Han, Y., Zhuang,
 653 M., Wang, M., Zhang, J., Zhang, X., Dusek, U., and Cao, J.: Size distribution and mixing
 654 state of refractory black carbon aerosol from a coastal city in South China, *Atmospheric*
 655 *Research*, 181, 163-171, <https://doi.org/10.1016/j.atmosres.2016.06.022>, 2016.
 656 Wang, Y., Liu, F., He, C., Bi, L., Cheng, T., Wang, Z., Zhang, H., Zhang, X., Shi, Z.,
 657 and Li, W.: Fractal Dimensions and Mixing Structures of Soot Particles during
 658 Atmospheric Processing, *Environmental Science & Technology Letters*, 4, 487-493,
 659 10.1021/acs.estlett.7b00418, 2017c.
 660 Wang, Y., Hu, M., Lin, P., Tan, T., Li, M., Xu, N., Zheng, J., Du, Z., Qin, Y., Wu, Y.,
 661 Lu, S., Song, Y., Wu, Z., Guo, S., Zeng, L., Huang, X., and He, L.: Enhancement in
 662 Particulate Organic Nitrogen and Light Absorption of Humic-Like Substances over
 663 Tibetan Plateau Due to Long-Range Transported Biomass Burning Emissions, *Environ*
 664 *Sci Technol*, 53, 14222-14232, 10.1021/acs.est.9b06152, 2019a.
 665 Wang, Y., Hu, M., Wang, Y., Zheng, J., Shang, D., Yang, Y., Liu, Y., Li, X., Tang, R.,
 666 Zhu, W., Du, Z., Wu, Y., Guo, S., Wu, Z., Lou, S., Hallquist, M., and Yu, J. Z.: The
 667 formation of nitro-aromatic compounds under high NO_x and anthropogenic VOC
 668 conditions in urban Beijing, China, *Atmospheric Chemistry and Physics*, 19, 7649-7665,
 669 10.5194/acp-19-7649-2019, 2019b.
 670 Wilcox, E. M., Thomas, R. M., Praveen, P. S., Pistone, K., Bender, F. A. M., and
 671 Ramanathan, V.: Black carbon solar absorption suppresses turbulence in the
 672 atmospheric boundary layer, *Proceedings of the National Academy of Sciences*, 113,
 673 11794-11799, 10.1073/pnas.1525746113, 2016.

674 Wu, Y., Wang, X., Tao, J., Huang, R., Tian, P., Cao, J., Zhang, L., Ho, K. F., Han, Z.,
675 and Zhang, R.: Size distribution and source of black carbon aerosol in urban Beijing
676 during winter haze episodes, *Atmos. Chem. Phys.*, 17, 7965-7975, 10.5194/acp-17-
677 7965-2017, 2017.

678 Zhang, F., Wang, Y., Peng, J., Chen, L., Sun, Y., Duan, L., Ge, X., Li, Y., Zhao, J., Liu,
679 C., Zhang, X., Zhang, G., Pan, Y., Wang, Y., Zhang, A. L., Ji, Y., Wang, G., Hu, M.,
680 Molina, M. J., and Zhang, R.: An unexpected catalyst dominates formation and radiative
681 forcing of regional haze, *Proceedings of the National Academy of Sciences*, 117, 3960-
682 3966, 10.1073/pnas.1919343117, 2020.

683 Zhang, R., Khalizov, A. F., Pagels, J., Zhang, D., Xue, H., and McMurry, P. H.:
684 Variability in morphology, hygroscopicity, and optical properties of soot aerosols
685 during atmospheric processing, *Proceedings of the National Academy of Sciences of*
686 *the United States of America*, 105, 10291-10296, 10.1073/pnas.0804860105, 2008.

687 Zhang, Y., Zhang, Q., Cheng, Y., Su, H., Li, H., Li, M., Zhang, X., Ding, A., and He,
688 K.: Amplification of light absorption of black carbon associated with air pollution,
689 *Atmospheric Chemistry and Physics*, 18, 9879-9896, 10.5194/acp-18-9879-2018,
690 2018a.

691 Zhang, Y., Su, H., Ma, N., Li, G., Kecorius, S., Wang, Z., Hu, M., Zhu, T., He, K.,
692 Wiedensohler, A., Zhang, Q., and Cheng, Y.: Sizing of ambient particles from a Single
693 Particle Soot Photometer measurement to retrieve mixing state of Black Carbon at a
694 Regional site of the North China Plain, *Journal of Geophysical Research: Atmospheres*,
695 123, 12778-12795, doi:10.1029/2018JD028810, 2018b.

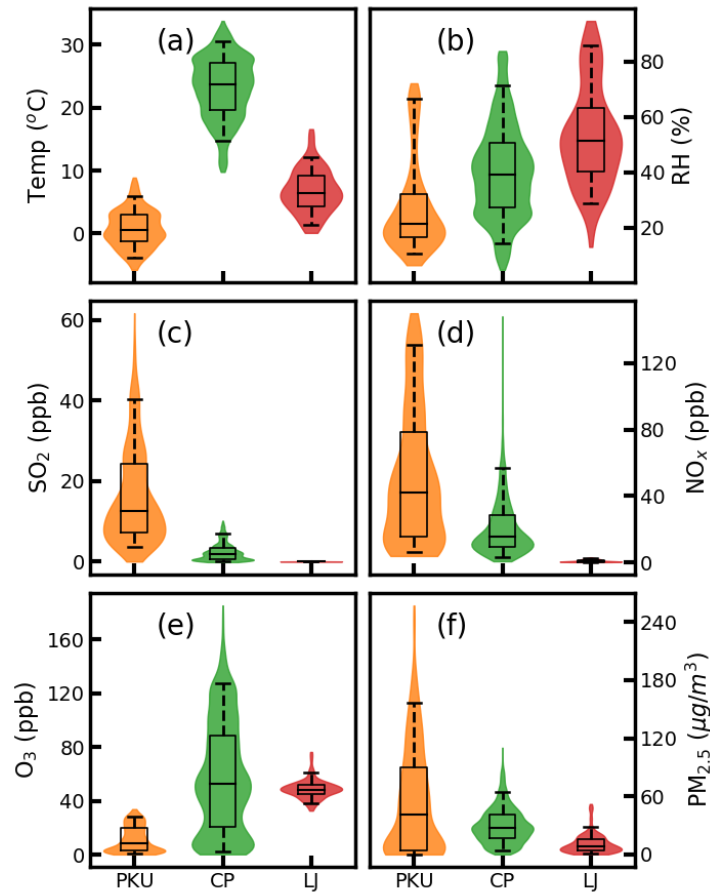
696 Zhao, G., Tao, J., Kuang, Y., Shen, C., Yu, Y., and Zhao, C.: Role of black carbon mass
697 size distribution in the direct aerosol radiative forcing, *Atmos. Chem. Phys.*, 19, 13175-
698 13188, 10.5194/acp-19-13175-2019, 2019.

699 Zhao, G., Hu, M., Fang, X., Tan, T., Xiao, Y., Du, Z., Zheng, J., Shang, D., Wu, Z.,
700 Guo, S., and Zhao, C.: Larger than expected variation range in the real part of the

701 refractive index for ambient aerosols in China, *Science of The Total Environment*, 779,
702 146443, 10.1016/j.scitotenv.2021.146443, 2021.
703 Zheng, J., Hu, M., Du, Z., Shang, D., Gong, Z., Qin, Y., Fang, J., Gu, F., Li, M., Peng,
704 J., Li, J., Zhang, Y., Huang, X., He, L., Wu, Y., and Guo, S.: Influence of biomass
705 burning from South Asia at a high-altitude mountain receptor site in China, *Atmospheric*
706 *Chemistry and Physics*, 17, 6853-6864, 10.5194/acp-17-6853-2017, 2017.

707

708



709

710 **Figure 1.** The measured distribution of (a) temperature, (b) RH, (c) SO₂, (d) NO_x, (e)
 711 O₃ and (f) PM_{2.5} for PKU (orange), CP (green) and LJ (red) sites, respectively. The box
 712 and whisker plots represent the 5th, 25th, 75th, and 95th percentiles. The width of the
 713 filled colors represents the probability distributions of the corresponding measured
 714 values.

715

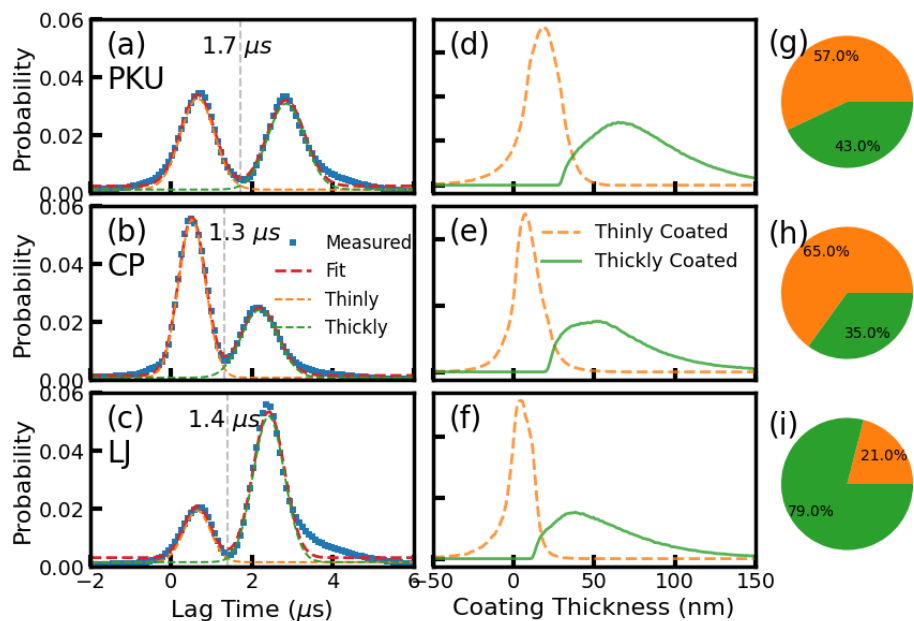


Figure 2. (a) The measured probability distribution of the lag time for the PKU site. Panel (d) shows the corresponding coating thickness distributions of fresh thinly coated (orange) and aged thickly coated (green) BC-containing aerosols. Panel (g) gives the number fraction of the fresh thinly coated (orange) and aged thickly coated (green) BC-containing aerosols. Panel (b), (e), and (h) are the corresponding values for the CP site. Panel (c), (f), and (g) give the results for LJ sites.

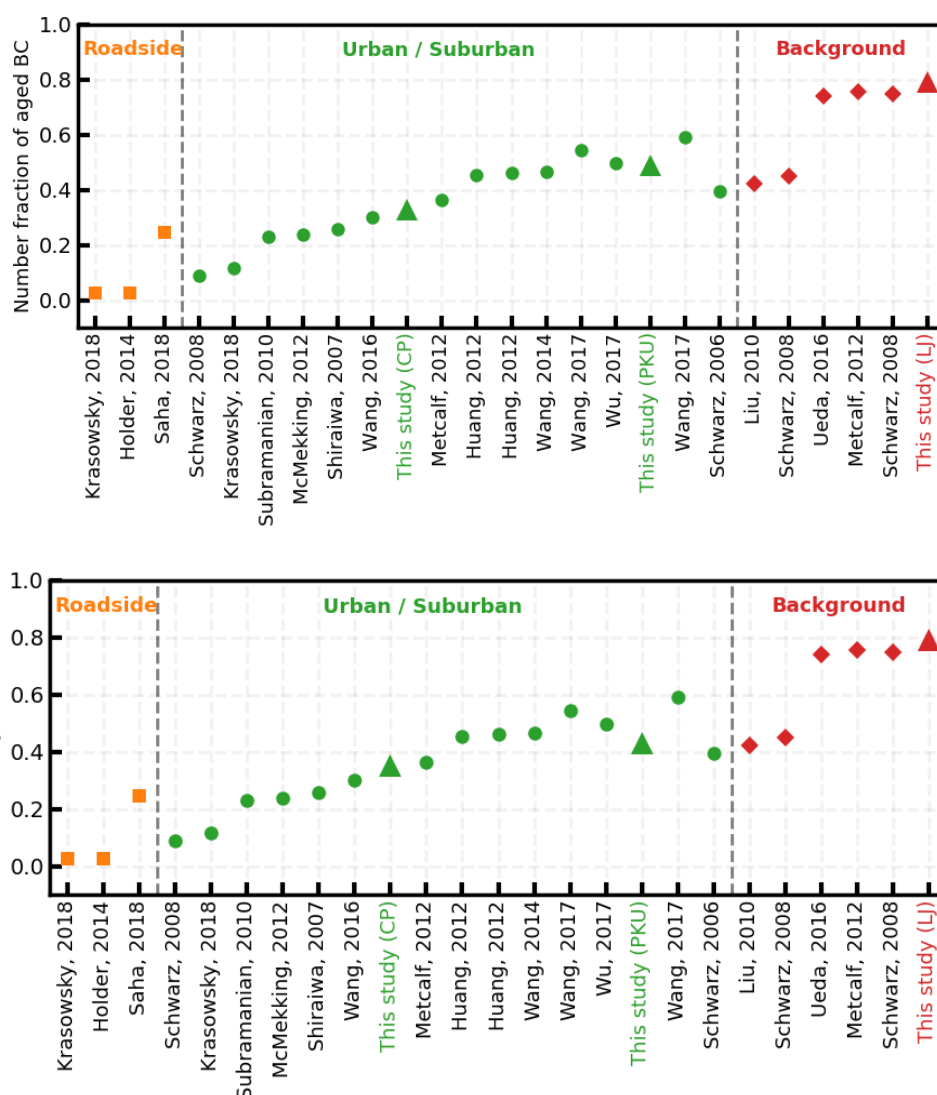


Figure 3. Measured number fraction of the aged thickly coated BC under different atmospheric environments based on literature. Our measured values are shown as triangles.

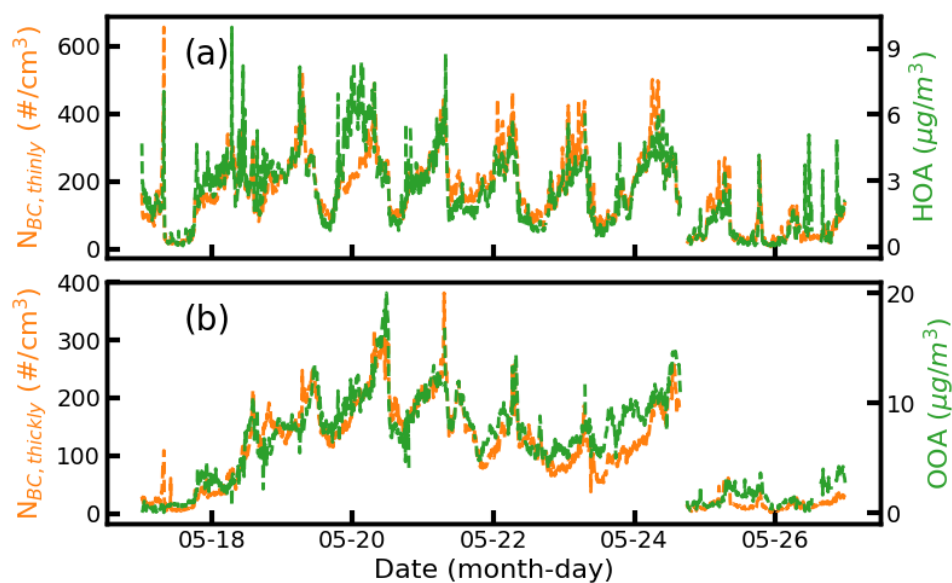


Figure 4. The time series of (a) the number concentration of the fresh thinly coated BC (orange) and the mass concentration of HOA (green), (b) the number concentration of aged thickly coated BC (orange), and the mass concentration of OOA (green) for the CP site.

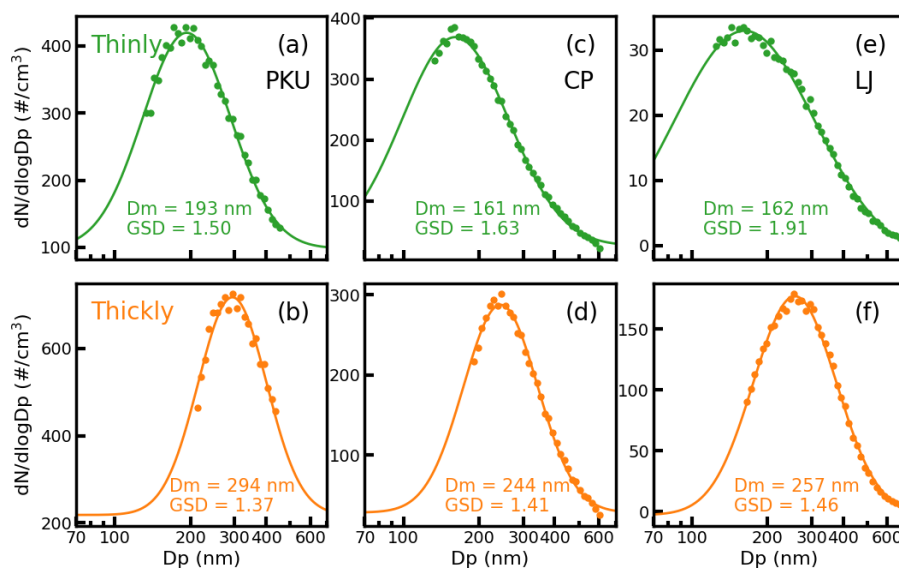
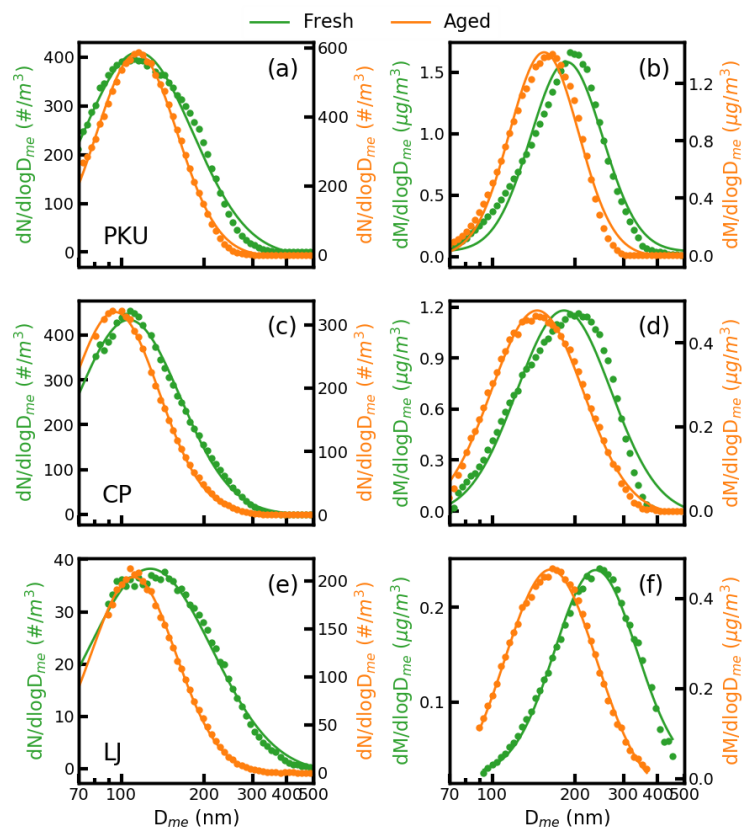


Figure 5. The number size distributions of the ~~fresh~~ thinly coated BC-containing aerosols at (a) PKU, (c) CP, and (e) LJ sites. Panels (b), (d), and (f) are the number size distributions of the aged thickly coated BC-containing aerosols for the PKU, CP, and LJ sites, respectively. The dots in the figure are the measurement results and the lines are the corresponding fit results with a log-normal distribution.



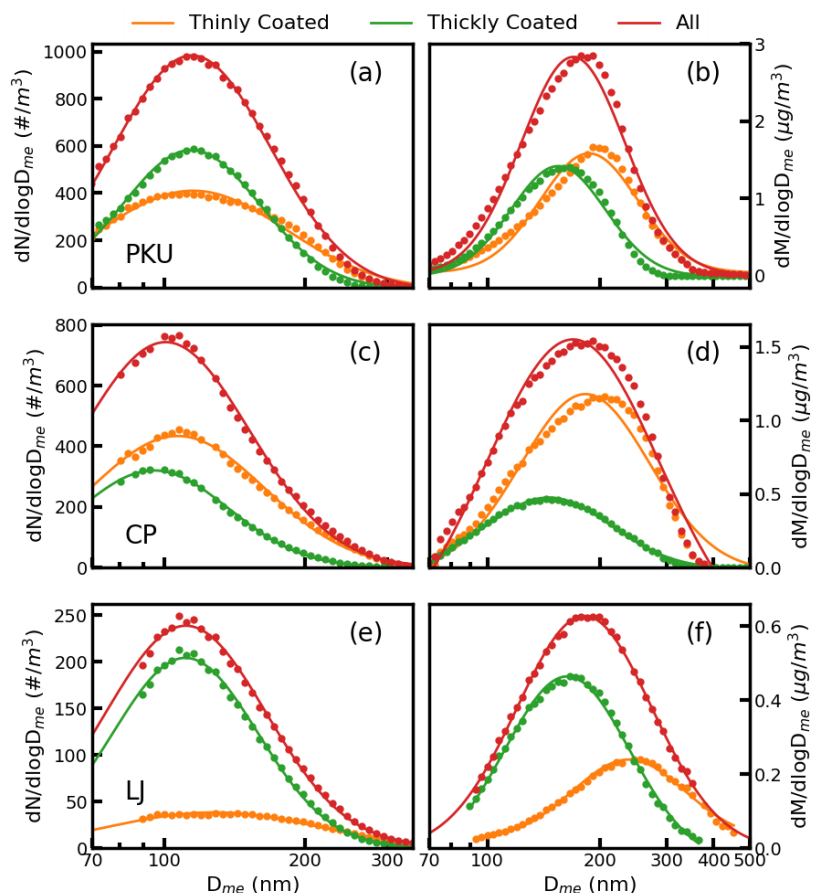


Figure 6. The BC core number size distributions of the fresh thinly coated (greenorange) and aged thickly coated (orangegreen), and overall (red) BC aerosols for the (a) PKU, (c) CP, and (e) LJ sites. Panel (b), (d) (f) show the BC core mass distributions of the fresh thinly coated (greenorange), and aged thickly coated (orange), and overall (red) BC aerosols for the PKU, CP, and LJ sites, respectively.

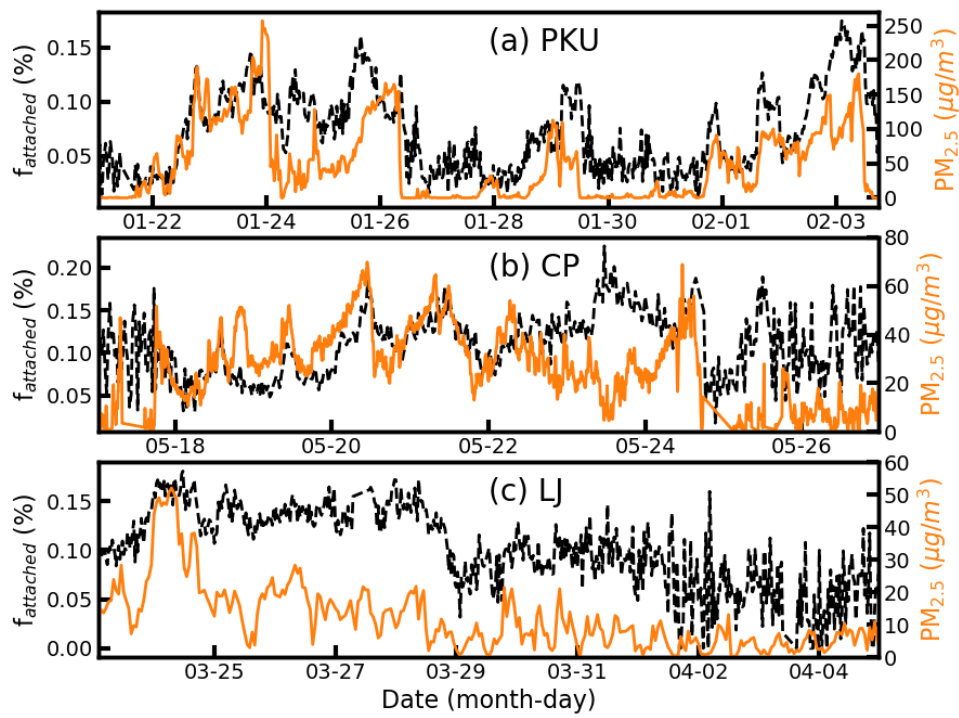
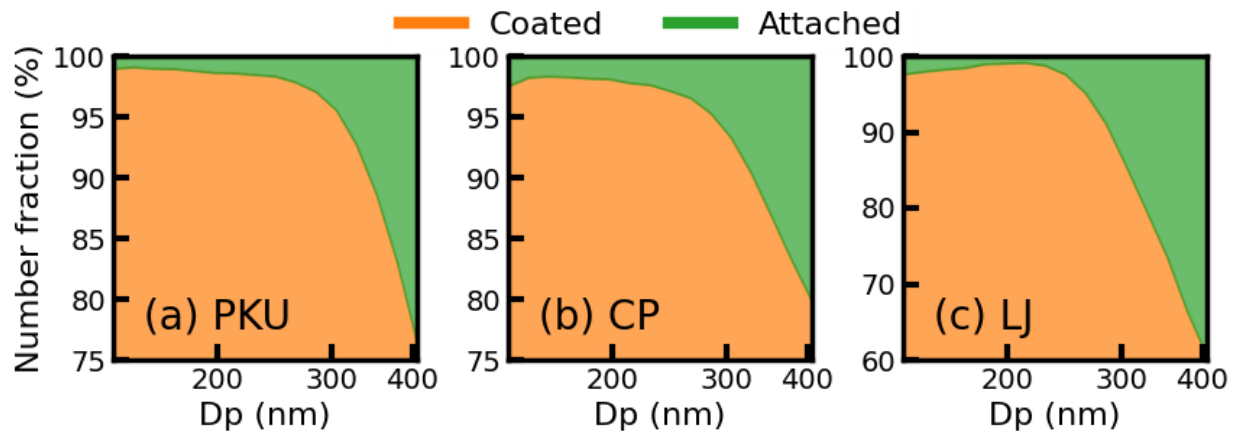


Figure 7. The time series of the number fractions of the attached BC (black) and PM_{2.5} mass concentrations (orange) for the (a) PKU, (b) CP, and (c) LJ sites.

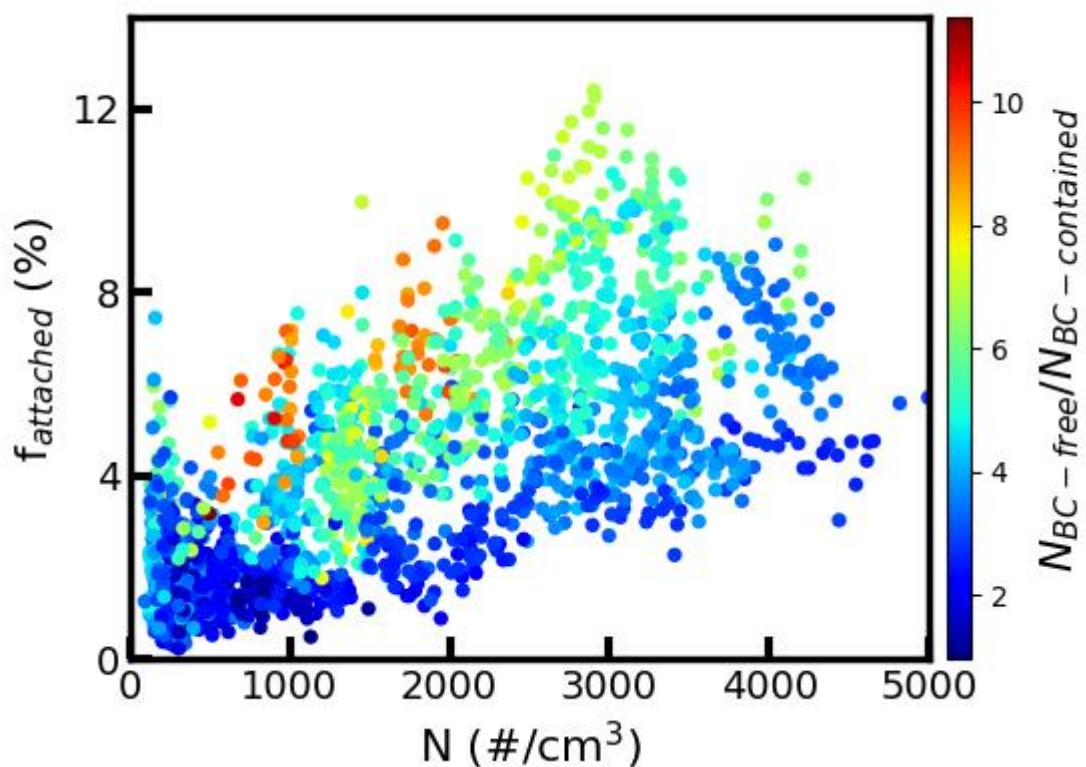
755



756

757 **Figure 8.** The number fractions of the coated and attached BC under different
758 diameters for the (a) PKU, (b) CP, and (c) LJ sites.

759



760

761 **Figure 9.** The number fractions of the attached BC aerosols under different total
 762 aerosol number concentrations for the CP sites. The filled colors represent the ratios
 763 between the BC-free aerosol number concentrations to the BC-containing aerosol
 764 number concentrations.

765

766 **Table 1.** The D_{me} and GSD values of the BC core at different sites.

Site	Value	Number Distribution			Mass Distribution ⁷⁶⁷		
		thinly coated	thickly coated	All	thinly coated	thickly coated	All
PKU	D_{me} (nm)	115	114	114	187	154	172
	GSD	1.58	1.40	1.47	1.35	1.34	1.37
CP	D_{me} (nm)	107	95	100	182	146	169
	GSD	1.53	1.45	1.51	1.48	1.47	1.47
LJ	D_{me} (nm)	127	111	112	238	163	181
	GSD	1.68	1.43	1.48	1.47	1.41	1.42